Supplementary Online Information (SOM)

Title: High concentrations of biological aerosol particles and ice nuclei during and after rain

Authors: J. A. Huffman[1,2*], A. J. Prenni[3*], P. J. DeMott[3], C. Pöhlker[2], R. H. Mason[4], N. H. Robinson[5], J. Fröhlich-Nowoisky[2], Y. Tobo[3], V. R. Després[6], E. Garcia[3], D. J. Gochis[7], E. Harris[2], I. Müller-Germann[2], C. Ruzene[2], B. Schmer[2], B. Sinha[2,8], D. A. Day[9], M. O. Andreae[2], J. L. Jimenez[9], M. Gallagher[5], S. M. Kreidenweis[3], A. K. Bertram[4*], U. Pöschl[2*]

Affiliations:

[1]Department of Chemistry & Biochemistry, University of Denver, 2190 E. Illif Ave., Denver, CO, 80208, USA.

[2]Max Planck Institute for Chemistry, P. O. Box 3060, D-55020, Mainz, Germany.

[3]Department of Atmospheric Science, Colorado State University, 1371 Campus Delivery, Fort Collins, CO, 80523, USA.

[4]Department of Chemistry, University of British Columbia, Room D223, 2036 Main Mall, Vancouver, BC, V6T1Z1, Canada.

[5]Centre for Atmospheric Sciences, University of Manchester, Simon Building, Oxford Road, Manchester, M139PL, UK.

[6]Institute for General Botany, Johannes Gutenberg University, Müllerweg 6, D-55099, Mainz, Germany.

[7]National Center for Atmospheric Research, PO Box 3000, Boulder, CO, 80307, USA.

[8]IISER Mohali, Department of Earth and Environmental Science, Sector 81, S. A. S. Nagar, Manauli PO, 140306, India.

[9]Cooperative Institute for Research in the Environmental Sciences and Department of Chemistry and Biochemistry, University of Colorado, Boulder, CO USA.

[*] Correspondence to: alex.huffman@du.edu (J. A. H.); anthony.prenni@colostate.edu (A. J. P.); bertram@chem.ubc.ca (A. K. B.); u.poschl@mpic.de (U. P.)

Supplementary Materials:

S1 Materials and Methods

S1.1 Meteorological and Leaf Moisture Measurements

Precipitation occurrence, rate and microphysical state (i.e., rain versus hail) were measured using a laser-optical disdrometer (PARticle SIze and VELocity 'PARSIVEL' sensor; OTT Hydromet GmbH, Kempton, Germany). Particle size is estimated from the magnitude of beam attenuation. Particle fall speed is determined from the duration of beam attenuation while overall precipitation rate and microphysical classification estimates are generated from a combination of the size and fall speed measurements. The sensor detects liquid hydrometeor particles ranging in size from 0.2 to 5 mm in diameter, solid hydrometeors ranging in size from 0.2 to 25 mm and provides estimates of particle velocities from 0.2 to 20 m/s.

S1.2 UV-APS

Aerosol sampling was performed with a volumetric flow of 5 $L \cdot min^{-1}$ (LPM) at ambient pressure and temperature, split within the instrument into a sample flow of 1.0 ± 0.1 LPM and a sheath flow of 4.0 ± 0.1 LPM (pressure difference feedback control). The instrument was controlled and the measurement data were recorded with an external computer connected via serial port using the manufacturer's Aerosol Instrument Manager software (TSI AIM; Shoreview, MN).

S1.3 WIBS

The waveband integrated bioaerosol sensor – model 4 (WIBS4; University of Hertfordshire, U.K.) is a dual channel single particle fluorescence spectrometer (Kaye et al., 2005; Foot et al., 2008; Gabey et al., 2010). The WIBS4 model is essentially the same as the WIBS3 model employed by Gabey et al. (2010), but with improved optics and electronics providing a more

precise signal. Baseline fluorescence is recorded by regularly measuring the internal fluorescence of the instrument when no particles are present. The increased precision of the model 4 WIBS allows for the detection of more weakly fluorescent particles than was possible using previous WIBS models.

A subset of the WIBS4 single particle data (8000 particles) was analyzed using hierarchical agglomerative cluster analysis using a group average distance metric. This clustering was analyzed in five dimensions which were z-score normalized before analysis: the three fluorescence channels, size, and asymmetry. A suitable solution was assessed by inspecting the coefficient of determination and the root mean squared distance between clusters for each (e.g. Robinson et al., 2011). Concentration time series for each cluster were established by comparing each of the remaining particles to the centroid of each cluster. Each time series was apportioned a fraction of the particles' count which was inversely proportional to the distance of the particle from each cluster centroid (expressed in number of standard deviations of the centroid).

S1.4 Filter and Impactor Aerosol Samples

S1.4.1 Sample Collection

S1.4.1.1 Cascade Aerosol Impactor (MOUDI)

The MOUDI sampler provided aerosol fractionation according to the following aerodynamic diameter size cuts (D_{50}, μm) (Marple et al., 1991):

Stage 1	18.0
Stage 2	10.0
Stage 3	5.6

Stage 4	3.2
Stage 5	1.8
Stage 6	1.0
Stage 7	0.56
Stage 8	0.32
Stage 9	0.18
Stage 10	0.10
Stage 11	0.056

Stage 1 is typically referred to as the pre-impactor, and stages 2-11 refer to stages in the MOUDI impactor. Because we are interested in large particles we refer to the pre-impactor as Stage 1 and list all stages as 1-11. Thus, the numbering scheme utilized here is shifted lower by one with respect to the common usage for MOUDI samplers.

MOUDI samples collected at the following times were analyzed by fluorescence microscopy and used for microscopic ice nucleation activation experiments as discussed in the manuscript:

M01 (dry period)	7/22 14:29 – 7/23 09:41	(1152 min.)
M10 (rain period)	8/2 05:55 – 8/3 05:55	(1440 min.)
M26 (rain period)	8/16 20:26 – 8/17 06:32	(606 min.)
M27 (dry period)	8/17 06:35 – 8/17 19:46	(791 min.)

Size distribution of ice nuclei shown in Figure 3C for dry periods are average of samples M1 and M27; Figure 3D for rain periods are average of samples M10 and M26. Corresponding time periods for UV-APS are identical to MOUDI sample periods.

99

100 ***S1.4.1.2 Glass Slide Impactor Samples***

101 Glass slide impactor samples collected at the following times are shown in Figures 3A and 3B
102 and discussed in the manuscript:

103	G09 (dry period)	7/31 12:17 – 12:49	(32 min.)
104	G21 (rain period)	8/3 23:56 – 8/4 0:27	(31 min.)

105

106 ***S1.4.1.3 Nuclepore® Filters***

107 Stacked filter samples collected at the following times are discussed in the manuscript:

108	S10 (dry period)	7/31 11:57 – 15:58	(241 min.)
109	S12 (dry period)	7/31 19:58 – 23:55	(237 min.)
110	S20 (rain period)	8/4 3:52 – 8:04	(252 min.)
111	S23 (rain period)	8/4 16:23 – 20:24	(261 min.)

112

113 ***S1.4.2 Fluorescence Microscopy***

114 In Fig. 3A and 3B an overlay of fluorescent emission from all three fluorescence microscope
115 channels (DAPI, GFP, TexasRed) onto a brightfield image of the same sample area is shown. For
116 comparability the exposure times of the individual fluorescence images in Fig. 3A and 3B were
117 set to the same values. The overlay image Fig. 3B is dominated by "blue-green" fluorescence
118 indicating strong emissions in the DAPI (λ_{ex} = ~360 nm, λ_{em} = ~460 nm) and GFP
119 (λ_{ex} = ~470 nm, λ_{em} = ~535 nm) channels. Blue-green fluorescence is characteristic for biological
120 material and mainly originating from protein and coenzyme fluorophores (Pöhlker et al., 2012).
121 In contrast "red-yellow" fluorescence is predominating in the overlay image in Fig. 3A

indicating strong emission in the TexasRed channel (λ_{ex} = ~560 nm, λ_{em} = ~630 nm). Red-yellow fluorescence is regarded to be somewhat characteristic/typical for mineral dust (Bozlee et al., 2005).

S1.5 Real-Time Ice Nucleation Measurements with CFDC

S1.5.1 IN Measurements

CFDC measurements were collected at the following times are shown in Figures 3E and 3F and discussed in the manuscript:

C01 (rain period)	8/2 10:27 – 17:57	(450 min.)
C02 (dry period)	8/17 16:27 – 23:47	(440 min.)

Periods C01 and C02 correspond to sub-periods during MOUDI samples M10 and M27, respectively.

References:

Bozlee, B. J., Misra, A. K., Sharma, S. K. and Ingram, M.: Remote Raman and fluorescence studies of mineral samples, Spectrochimica Acta Part a-Molecular and Biomolecular Spectroscopy, 61, 2342-2348, 10.1016/j.saa.2005.02.033, 2005.

Foot, V. E., Kaye, P. H., Stanley, W. R., Barrington, S. J., Gallagher, M. and Gabey, A.: Low-cost real-time multi-parameter bio-aerosol sensors, Proceedings of the SPIE - The International Society for Optical Engineering, 711601 (711612 pp.), 10.1117/12.800226, 2008.

Gabey, A. M., Gallagher, M. W., Whitehead, J., Dorsey, J. R., Kaye, P. H. and Stanley, W. R.: Measurements and comparison of primary biological aerosol above and below a tropical forest canopy using a dual channel fluorescence spectrometer, Atmospheric Chemistry and Physics, 10, 4453-4466, 10.5194/acp-10-4453-2010, 2010.

Kaye, P. H., Stanley, W. R., Hirst, E., Foot, E. V., Baxter, K. L. and Barrington, S. J.: Single particle multichannel bio-aerosol fluorescence sensor, Optics Express, 13, 3583-3593, 2005.

Marple, V. A., Rubow, K. L. and Behm, S. M.: A microorifice uniform deposit impactor (MOUDI) - description, calibration, and use, Aerosol Sci. Technol., 14, 434-446, 10.1080/02786829108959504, 1991.

Pöhlker, C., Huffman, J. A. and Pöschl, U.: Autofluorescence of atmospheric bioaerosols - fluorescent biomolecules and potential interferences, Atmospheric Measurement Techniques, 5, 37-71, 10.5194/amt-5-37-2012, 2012.

Robinson, N. H., Newton, H. M., Allan, J. D., Irwin, M., Hamilton, J. F., Flynn, M., Bower, K. N., Williams, P. I., Mills, G., Reeves, C. E., McFiggans, G. and Coe, H.: Source attribution of Bornean air masses by back trajectory analysis during the OP3 project, Atmospheric Chemistry and Physics, 11, 9605-9630, 10.5194/acp-11-9605-2011, 2011.

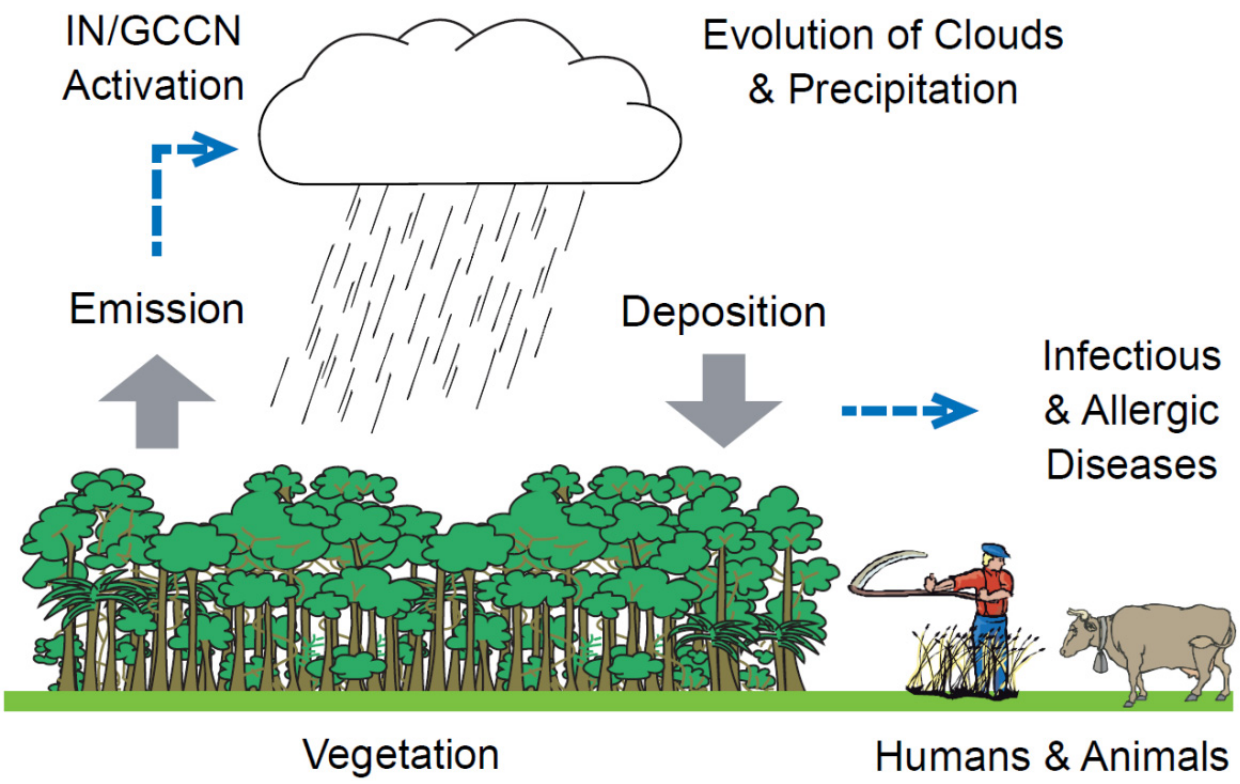

Figure S1: Coupling and effects of biological aerosol particles and precipitation: rain can enhance bioparticle emissions (rain splash, active wet discharge, etc.); bioparticles serving as ice nuclei or giant cloud condensation nuclei (IN/GCCN) can influence the evolution of clouds and precipitation; deposition of pathogenic and allergenic species can trigger human, animal and plant diseases.